Phase separation and collapse in almost density matched depletion induced colloidal gels in presence and absence of air bubbles

Thompson, Emma; Declercq, Marc; Saveyn, Pieter; Guida, Vincenzo; Robles, Eric S. J.; Britton, Melanie

DOI:
10.1016/j.jcis.2020.07.148

Document Version
Peer reviewed version

Citation for published version (Harvard):
Thompson, E, Declercq, M, Saveyn, P, Guida, V, Robles, ESJ & Britton, M 2020, 'Phase separation and collapse in almost density matched depletion induced colloidal gels in presence and absence of air bubbles: an MRI imaging study.', *Journal of Colloid and Interface Science*, vol. 582, no. A, pp. 201-211. https://doi.org/10.1016/j.jcis.2020.07.148

Phase separation and collapse in almost density matched depletion induced colloidal gels in presence and absence of air bubbles: an MRI imaging study.

Emma S. Thompson[a,d], Marc Declercq[b], Pieter Saveyn[b], Vincenzo Guida[b], Eric S. J. Robles[c] and Melanie M. Britton[a*]

[a] School of Chemistry, University of Birmingham, Birmingham, B15 2TT, UK

[b] Procter & Gamble Brussels Innovation Center, 1853 Strombeek Bever, Temselaan 100, Belgium

[c] Procter & Gamble Company, Newcastle Innovation Centre, Newcastle-Upon-Tyne NE12 9TS, UK

[d] current address: BASF SE, Carl-Bosch-Strasse 38, 67056 Ludwigshafen am Rhein, Germany

* Corresponding author; Tel. +44 (0)1214144391; Email: m.m.britton@bham.ac.uk

Abstract:

Hypothesis: Vesicle-polymer dispersions are found in drug-delivery systems and consumer products but undergo phase separation. Previous studies of phase separation have focussed on systems with high density differences between continuous and vesicular phases. In this study, we investigate phase separation in vesicle-polymer mixtures with very small density differences, in the presence and absence of air bubbles.

Experiments: Magnetic resonance (MR) imaging, X-ray Computed Tomography and rheological measurements are reported which characterise the properties and stability of vesicle suspensions composed of the cationic surfactant, diethylesterdimethyl ammonium chloride, mixed with non-adsorbing polymer. ^{1}H T_2 MR relaxation images are employed to observe phase separation, for a range of vesicle-polymer mixtures, which are analysed using Moran's *I* spatial autocorrelation to quantify the extent and rate of phase separation.

Findings: It was found that in presence of air bubbles, phase separation follows a compression/collapse mechanism, typical of colloidal gels with large density differences between the phases. Without air bubbles, phase separation develops through the formation of tiny cracks and fractures in the samples. MRI enabled visualisation of the evolution of phase separation inside highly turbid samples. The rate of phase separation was found to generally increase with increasing polymer concentration and decrease with increasing vesicle volume fraction.

Keywords: Moran's I, DEEDMAC, polyDADMAC, MRI, T_2 MR relaxation time images, phase separation, X-ray CT, yield stress, air bubbles.

1. Introduction

Colloidal suspensions are kinetically stable and, over time, undergo phase separation because of density differences between the colloidal particles and the continuous phase [1]. Adding polymer to a colloidal suspension can cause suspended particles to aggregate and form a colloidal gel [2], either

through bridging flocculation, by interacting directly with the particles, or through depletion flocculation [3]. Depletion flocculation occurs because the small polymer coils cannot approach within a certain distance of the large colloidal particles and, therefore, each colloidal particle possesses a depletion layer [4]. When the large particles approach and the depletion layers overlap, there is more space for the small polymer particles in solution, therefore, it is entropically favourable for the large particles to aggregate [4]. If the particle volume fraction is sufficiently high, a space spanning gel network can form. The resulting gel network has a percolated, bi-continuous structure which will eventually collapse, because of the combination of attraction forces and gravity, into particle-rich and particle-poor phases [3, 5]. While, the link between gelation and phase separation in colloidal systems is complex, understanding phase separation and gel collapse is of critical importance for the use of colloidal suspensions in many consumer products, food and medicine [5].

There have been numerous studies of gelation and phase separation in hard sphere colloidal systems [1, 2, 5-7]. These studies have often described gelation as the result of an arrested spinodal decomposition during phase separation. [3, 5] Gel compression and collapse leads to two phases with different densities layering one over the other, which is explained by the balance between gravitational and elastic forces [6], and the poro-elastic model predicts that the colloidal gel is compressed by gravity, expelling the continuous phase, via filtration flow. The rate of phase separation is controlled by the porosity of the gel network, while the extent of compression depends on the elastic modulus of the gel.

Evidence for gelation in these colloidal systems is typically acquired from rheological measurements, as well as observing gel behaviour close to objects which disrupt the gel network.[6] Disruptions of the gel network have been shown to cause the development of particle-poor cracks in the particle-rich phase [6]. Most of the experimental studies on colloidal gel phase separation are made using

mono-disperse polystyrene or poly(methyl methacrylate) microspheres as colloidal particles. However, suspensions of mono-disperse, hard colloidal particles are not representative of many industrially relevant systems.

One type of colloidal suspension commonly found in drug delivery systems and consumer products are vesicle dispersions [8]. In particular, vesicles formed with the cationic surfactant diethylesterdimethyl ammonium chloride (DEEDMAC) are used on a large global scale as biodegradable fabric enhancer [9]. Vesicle dispersions are frequently mixed with non-adsorbing polymer to form transient gel networks in order to improve rheological properties, such as flowability and dispensability [3, 10]. Vesicles are internally filled with an aqueous phase that is isotonic with the external continuous phase and this makes the density difference and thus the gravitational forces very small compared to microgel particles. Furthermore, the polydispersity and softness of the vesicles further complicate gelation and phase separation processes. For example, polydispersity might lead to size fractionation during phase separation [3]. This additional complexity means phase separation and gelation in vesicle dispersions could be different to that of microsphere suspensions [3].

Phase separation and gelation of DEEDMAC vesicle dispersions mixed with non-adsorbing polymer, such as poly-diallyldimethyl ammonium chloride (polyDADMAC), have, previously, been studied at low to medium volume fraction (ϕ = 0.05 – 0.30), high polymer concentrations (0.3 – 2.0 %wt) and polymer to particle size ratios (R_g/a) of 0.09 [3, 10] and 0.27 [10]. The density difference between continuous phase and vesicles, in such systems, is 50 kg m^{-3} [11]. All these variable factors affect the strength of the depletion interactions and, therefore, the strength of the gel network. It was found that, in the absence of polymer, the dispersion is stable over a few weeks [10]. Yet, in the presence of polymer, the dispersions separate into vesicle-poor and vesicle-rich phases in a matter of hours. At vesicle volume fraction (ϕ) > 0.15, gel networks form, via arrested spinodal decomposition, which were

visualised using confocal microscopy [3, 10]. The rate of gel collapse in these systems was found to increase with polymer concentration, which is unexpected, because higher polymer concentrations lead to stronger gels that are typically more resistant to the effects of gravity [3, 10]. Increasing polymer concentration was shown to increase the porosity and permeability of the gel network which makes the network more tenuous and it collapses faster [10]. This was further investigated by measuring the height of the particle-rich phase over time and fitting the reduction in height of these gels to a poroelastic model [3], which states that gel collapse is dependent on gravity, viscous drag and elastic forces within the material [12].

Furthermore, in other systems, such as TEQ (triethanolamine-based esterquat) vesicle dispersions mixed with a non-adsorbing polymer (Specific dextrin derivative (SDD)) studied by Miyajima et al. [13], the relationship between rheology and physical stability has been investigated. These systems were studied at mass fraction (w = 0.04 – 0.16), high polymer concentrations (0.04 – 3.2 %wt) and polymer to particle size ratios (R_g/a) of 0.16 but no information was provided on vesicle volume fraction. They found that it is possible to produce a stable depletion gel with reasonable viscosity for intermediate polymer and esterquat concentrations. However, the stability of these systems is not well understood.

Elastic forces within colloidal suspensions undergoing phase separation have been linked to the formation of particle-poor regions within a particle-rich phase [6, 14]. The progression of phase separation in previous studies of DEEDMAC vesicle dispersions [3, 10] has been modelled using the height of the vesicle-rich phase as a means of monitoring the progress of phase separation. While the development of heterogeneity within the vesicle-rich phase has not been investigated, it has been shown that vesicle-poor voids form in the vesicle-rich phase suggesting that imaging techniques may be able to provide more insight [15]. Furthermore, Tanaka et al. [16, 17] have shown that phase separation into colloid-rich and colloid-poor structure can develop even in the absence of gravitational forces just as a consequence of the attractive forces between the colloids. Depending on the relation of the deformation rate, generated by phase separation itself, to the bulk and shear mechanical

relaxation rates, a transient network demonstrates viscoelastic and elastic properties, leading to a liquid-like fracture of the network during shrinking. However, in the experiments quoted by Koyama and Tanaka [16] the samples were sandwiched between two cover glasses and, thus, were quasi-two-dimensional. This enabled from one side the visualization of phase separation through an opaque sample and on the other side eliminated the effect of gravitational forces.

Previously, magnetic resonance imaging (MRI) has enabled sedimentation and creaming to be observed, non-invasively, in opaque systems [5, 14, 18-25]. Also, MRI has been widely used to characterise sedimentation and creaming in a wide variety of systems including polymer particles [5, 14, 19, 20, 22], paliperidone palmitate particles [25], glass beads [19] and rayon fibres [24], as well as being used to study application specific systems such as crude oil [21], biodiesel [18] and moisturising creams [23]. MRI has provided a way of investigating the structure of the colloid-rich phase [14] and, through image analysis, using techniques like Moran's I, phase separation has been quantified when the local colloid volume fraction is not only dependant on the gravitational field [15].

In this paper, MRI, X-ray Computed Tomography (X-ray CT) and rheological measurements have been used to characterise the properties and stability of suspensions of almost density matched DEEDMAC vesicles mixed with non-adsorbing polymer to form transient colloidal gels. The vesicle volume fractions used in this study (ϕ = 0.3 - 0.5) are in the range typically found in consumer products, but are higher than those previously studied [3, 10] and the polymer concentrations used are lower than those previously studied [10, 26]. In such systems, the density difference between vesicles and continuous phase is expected to be very small, as the vesicles are filled with the continuous phase. Phase separation, under this extremely small density difference, is studied herein. The gel stability is assessed, in the presence and absence of air bubbles, and at different gel strengths. ^{1}H T_2 MR relaxation images are used to observe phase separation, and, in certain cases, Moran's I is employed to quantify the extent and rate of phase separation [15].

2. Materials and Methods

2.1. Sample Preparation

Aqueous dispersions of DEEDMAC vesicles, with a vesicle volume fraction (ϕ) of 0.5, were prepared according to an extrusion process with an apparatus similar to the one described previously [27]. Dispersions of lower volume fraction (ϕ = 0.4 and ϕ = 0.3) were obtained by isotonically diluting the ϕ = 0.5 dispersion with 450 ppm formic acid (Sigma). Volume fraction was measured according to the procedure previously described in [26]. Vesicles had typical sizes ranging from 100 nm - 5 µm. X-ray scattering measurements, cited in supplementary information (Figure S3), do not show Bragg reflection peaks, indicating the presence of mainly unilamellar vesicles with a bilayer thickness of 4.70 Å.

Vesicle dispersions were thoroughly mixed with an aqueous solution of the poly-diallyldimethyl ammonium chloride (poly-DADMAC) (M_w = 150000 g mol^{-1}) polymer, Merquat 100 (Lubrizol), giving final polymer concentrations of 0 - 0.25 % wt. The radius of gyration of this polymer is approximately 30 nm. For MR imaging, samples (ϕ = 0.3 - 0.5 and [polymer] = 0 - 0.25 %wt) were prepared under air or under vacuum, stored in 20 mm (outer diameter) glass test tubes (Cole-Parmer Instrument Co.) and imaged over 5 weeks. The height of each sample was 5 cm. For X-ray CT and rheology measurements, fresh samples were prepared under air.

2.2. MRI Experiments

MRI data were collected on a Bruker DMX 300 spectrometer equipped with a 7 T vertical wide-bore superconducting magnet, operating at a proton resonance frequency of 300.13 MHz with micro2.5 imaging gradients and 25 mm ^{1}H radio frequency (RF) bird cage coil (WB40 probe). All experiments were recorded at 293 ± 0.3 K, which was maintained by the temperature of the water-cooled micro2.5 gradient coils. RF pulses were calibrated for each sample. Vertical ^{1}H magnetic resonance (MR)

images of water in the vesicle dispersion were acquired using the spin-echo imaging sequence RARE (Rapid Acquisition with Relaxation Enhancement) [28]. Vertical MR images were acquired with a 1 mm slice thickness, 256 × 128 pixel matrix and field of view of 4.5 × 2.25 cm^2. T_2 MR relaxation maps were produced from 16 echo images with an echo time of T_E = 7 ms and a RARE factor of 16, leading to echo times ranging from 60 - 1740 ms. A repetition time of T_R = 10 s was used. All MRI data were analysed using *Prospa* [29]. In all MR images, a systematic variation in T_2 relaxation time is observed across the sample, which was removed as described in the Supplementary information and using the images (Figure S1) [30]. T_2 MR relaxation time maps were analysed using Moran's I [15, 31], which is a measure of spatial autocorrelation. Moran's I can vary from 1, for perfect correlation (where features are 'fully' clustered), to –1, for perfect alternation (where features are spaced periodically), and a Moran's I value of 0 represents a random distribution [15]. The Moran's I value was calculated for each image in Matlab [32] using equation 1, where N is the number pixels in the image, W_{ij} is a weight matrix defining spatial closeness, $X_{i/j}$ is the T_2 at pixel (i/j) and $\bar{X}$ is the mean T_2 for the image.

$$I = \frac{N}{\sum_i \sum_j W_{ij}} \frac{\sum_i \sum_j W_{ij} C_{ij}}{\sum_i (X_i - \bar{X})^2} = \frac{N}{\sum_i \sum_j W_{ij}} \frac{\sum_i \sum_j W_{ij} (X_i - \bar{X})(X_j - \bar{X})}{\sum_i (X_i - \bar{X})^2} \quad (1)$$

In our analysis, any pixels with a value of T_2 = 0 ms (and hence outside the sample) were set to equal the mean of the image so these would not contribute to the value of Moran's I. More details on the implementation of this analysis can be found elsewhere [15].

2.3 X-ray Computed Tomography

Vesicle-polymer mixtures (ϕ = 0.3 – 0.5 and [polymer] = 0 – 0.25 %wt) were placed into plastic cryogenic storage tubes (inner diameter = 9.4 mm, VWR), shaken, left to stand for 24 hrs and scanned using a Bruker Skyscan1172 micro-computed tomography system. A maximum X-ray energy of 50 kV was used, with 5 W beam power, 800 ms exposure per projection, a 0.5 mm aluminium filter and

14.87 µm pixel size. Data were reconstructed and then a volume of interest (VOI) was extracted using CTAn (Bruker). The VOI was chosen to include the whole of the vesicle-polymer dispersion but exclude the sample tube. Images were viewed and 3D representations were constructed using Image J [33].

2.4 Yield stress measurements

Rheology measurements of vesicle polymer mixtures (ϕ = 0.3 – 0.5 and [polymer] = 0 – 0.25 %wt) were conducted on a AR-G2 rheometer (TA instruments) using a cone and plate geometry (equipped with a 2˚ stainless steel cone, of 60mm diameter and 50 µm gap). Steady-state flow experiments were performed starting at a shear rate of 10 s^{-1} and reducing the shear rate to 10^{-5} s^{-1}, with 10 points per decade, logarithmically spaced. Data were acquired for a sample time of 30 s and at least three consecutive measurements were made at each point. The shear rate-shear stress (flow) curves were fitted, between 0.01 and 10 s^{-1}, to the Herschel-Bulkley equation (equation 2) where σ_0 is the yield stress, σ is the shear stress, $\dot{\gamma}$ is the shear rate, K is a measure of viscosity and n is the power law exponent [34]. Typical fits can be found in the supplementary information figure S2 and table S1.

$$\sigma = \sigma_0(1 - e^{-\dot{\gamma}}) + K\dot{\gamma}^n \quad (2)$$

2.5 Density measurements

The density of vesicles bilayer as a function of temperature was measured according to the procedure described in [35] and can be found in the supporting information.

3. Results

3.1 Bulk measurements

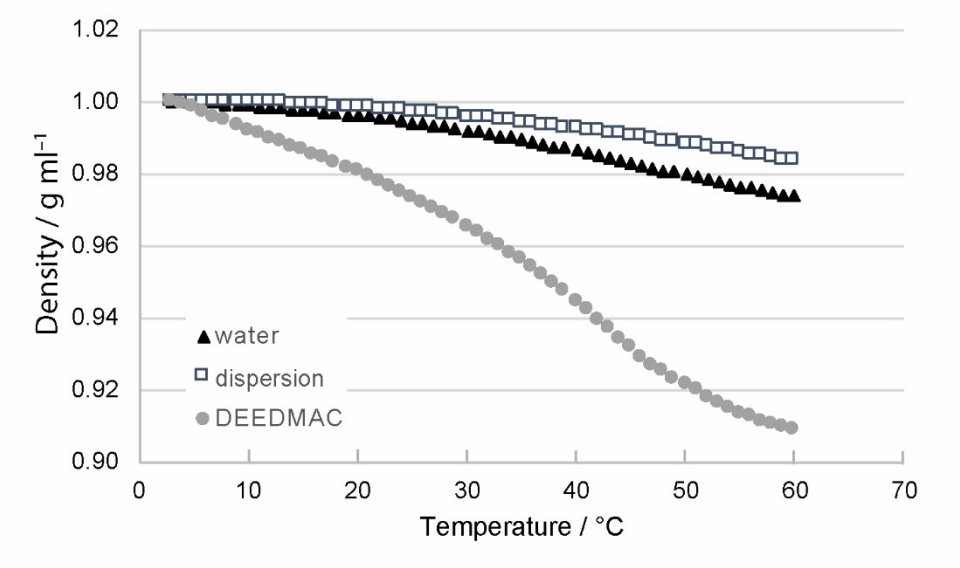

Figure 1: Graph of bulk density for a DEEMAC bilayer and a vesicle dispersion, compared with water, over a temperature range 3 – 60 °C

The density difference between a vesicle and the continuous phase depends on the vesicle size, the bilayer thickness and the number of bilayers. Figure 1 shows the density of a DEEDMAC bilayer and vesicle dispersion. At 20 °C, the density difference between the vesicle bilayer and the continuous aqueous phase is 16 kg m^{-3}. A vesicle dispersion is typically rather polydisperse, both in size and lamellarity. However, based on SAXS data (see supplementary information Figure S3) it can be assumed that the number of bilayers of the used dispersions was close to 1 and the bilayer thickness was derived from the same spectrum and estimated to be 4.7 nm. For example, a unilamellar vesicle of 250 nm radius, with a bilayer thickness of 4.7 nm, filled and surrounded by a solution that is 16 kg m^{-3} heavier than the bilayer, would have a density difference of less than 1 kg m^{-3}. This small difference is explained by the small difference in density, between the bilayer and the continuous phase, and by the small volume fraction (5% in the example) of the bilayer versus the entire vesicle volume.

Yield stress measurements were used to determine the gel strength of vesicle-polymer mixtures over the range ϕ = 0.3 – 0.5 and polymer concentrations = 0 – 0.25 %wt (figure 2). It was found that the yield stress values for these mixtures were very low (< 0.1 Pa) and that yield stress scales with

increasing ϕ and [polymer]. The dependence of the yield stress on ϕ and [polymer] was modelled using equation 3, where *k* is a constant and α and β are power law exponents [6, 7, 36].

$$\sigma_0 = k\,\phi^{\alpha}\,[\text{polymer}]^{\beta} \tag{3}$$

Values of α = 2.71 and β = 0.66 were determined using multicomponent linear regression. The data do not fit this model perfectly and the value of β = 0.66 is lower than the expected values of β = 2 for polymer concentrations approaching the overlap concentration [7]. It is, however, worth noting here that the volume fractions of the system were measured before polymer addition and it is expected that vesicles shrink slightly on polymer addition due to osmotic effects [30].

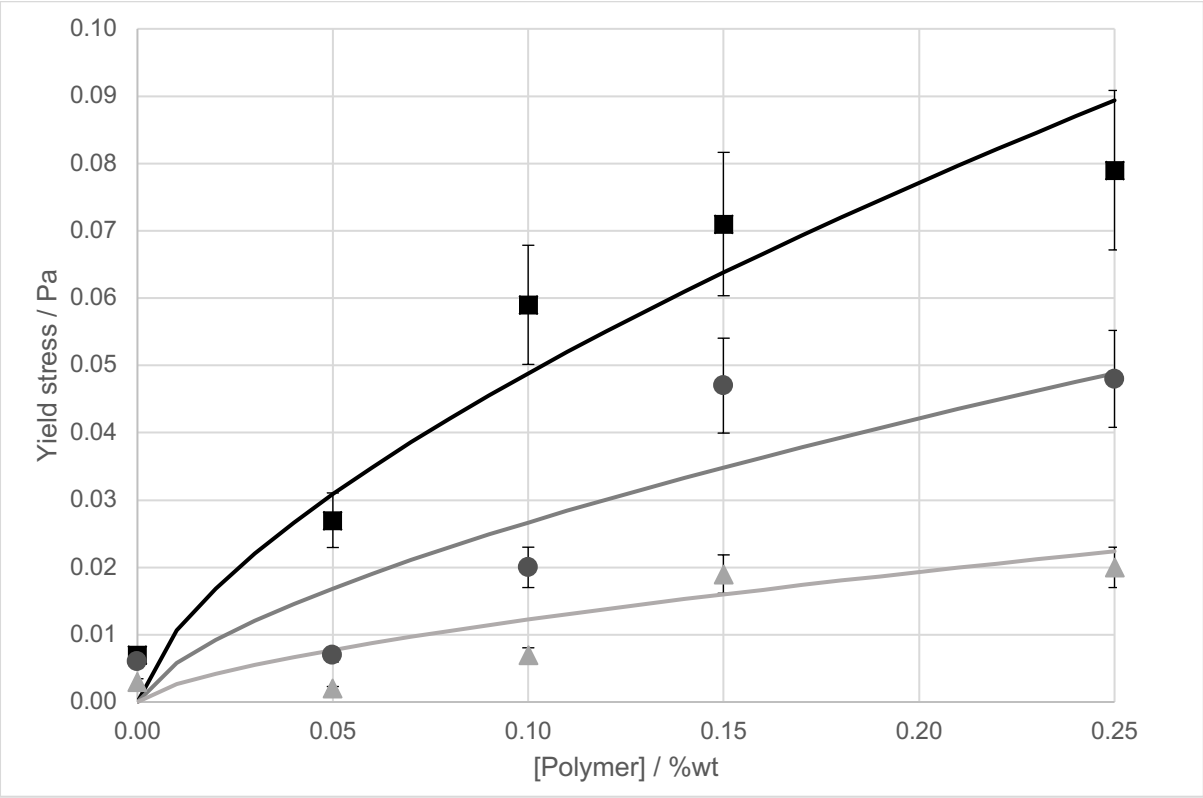

Figure 2: a) Plot of yield stress against polymer concentration for a range of vesicle-polymer mixtures at ϕ = 0.3 (grey triangles), ϕ = 0.4 (dark grey dots) and ϕ = 0.5 (black squares). The lines are a fit to the data using equation 3: yield stress = $k\,\phi^{\alpha}$ [polymer]$^{\beta}$ with *k* = 1.46, α = 2.71 β =0.66, for the mixtures at ϕ = 0.3 (grey solid line), ϕ = 0.4 (grey dashed line) and ϕ = 0.5 (black dashed line).

3.2 Phase separation in samples produced under air

Figure 3 shows extracted slices from X-ray CT images of a range of vesicle-polymer mixtures. From the X-ray CT images in Figure 3, it is apparent that concentrated vesicle-polymer mixtures (ϕ =0.5 for [polymer] = 0.25, 0.15, 0.10 %wt and ϕ = 0.4 for [polymer] = 0.25, 0.15 %wt) are able to trap air bubbles for up to 24 hrs. In these samples, typical air bubble sizes were found to be 350 µm (for mixtures at ϕ = 0.5 and [polymer] = 0.25 %wt), 200 µm (for mixtures at ϕ =0.5 and [polymer] = 0.15 %wt or 0.10 %wt; and at ϕ =0.4 [polymer] = 0.25 %wt) and 150 µm (for mixtures at ϕ =0.4 and [polymer] = 0.15 %wt). This demonstrates that vesicle-polymer mixtures, that have sufficient high yield stress, can suspend air bubbles, at least temporarily.

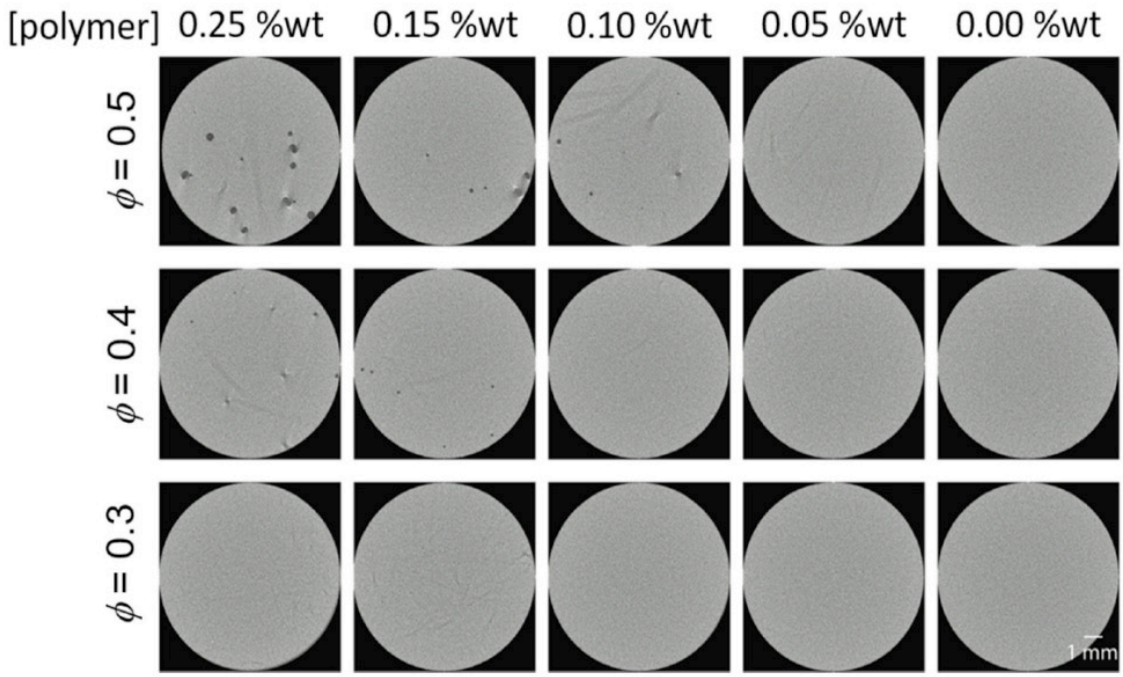

Figure 3: Slices from X-ray CT images of vesicle-polymer mixtures with ϕ = 0.3 – 0.5 and polymer concentrations = 0 – 0.25%wt at t = 24 hrs.

Figure 4a shows a time series of T_2 MR relaxation maps for a vesicle-polymer mixture (ϕ = 0.5 [polymer] = 0.25 %wt) containing air bubbles, which rise upwards over time. The image at t = 0 shows a T_2 of approximately 480 ms over most of the sample with some small, localised regions of low T_2 (T_2 < 300 ms) randomly distributed through the sample. The areas with T_2 = 480 ms were attributed to the

vesicle dispersion and the areas of lower T_2 were attributed to the air bubbles. In the later images (t = 2 – 12 hrs), regions of higher T_2 (T_2 > 600 ms) can be seen. These were attributed to regions containing fewer vesicles, which have the effect of shortening the T_2 relaxation time [15]. The air bubbles do not appear as regions of zero signal because the air bubbles are approximately 300 µm in diameter and, therefore, smaller than the slice thickness (1 mm). However, they could be directly visualised by X-ray CT (figure 4c). From the MR images, it can be seen that the air bubbles rise over time, as a result of gravity, and that, as they rise, vertical regions of high T_2 (T_2 > 600 ms) are observed, indicating the formation of vesicle-poor regions in the wake of the bubble. This can be most easily observed in the case of the circled air bubble in figure 4a. By monitoring this bubble over time, by plotting the T_2 relaxation time along its direction of travel (figure 4b), its trajectory and velocity was determined. Initially, its position was 1.7 cm at t = 0, and rose to a position of 2.1 cm at t = 12 hr. From this, the velocity of the air bubble was calculated to be 0.03 cm hr^{-1}. What can also be observed in figure 4 is a region of high T_2, in the wake of the rising air bubble, indicating a direct relationship between the rising air bubble and the formation of vesicle-poor regions.

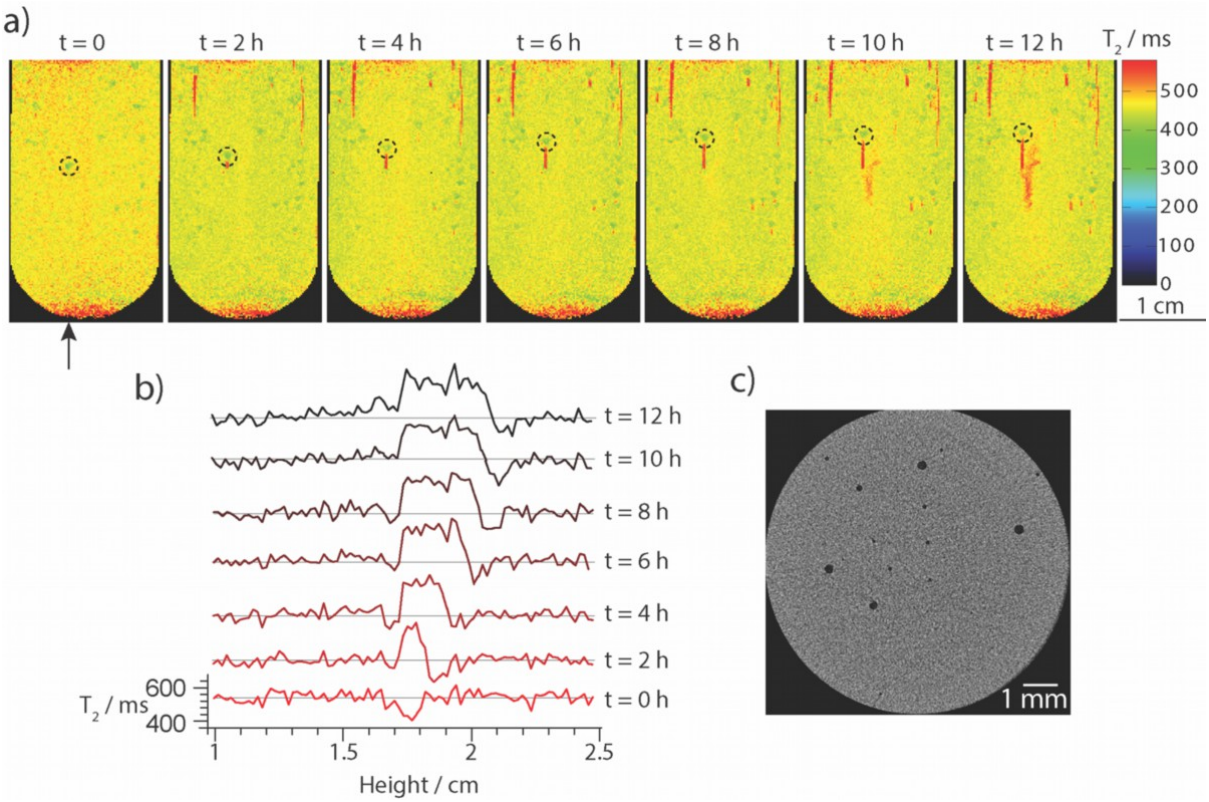

Figure 4: a) ^{1}H T_2 MR relaxation time maps of a vesicle-polymer mixture (ϕ = 0.5 [polymer] = 0.25 %wt) containing air bubbles. The position of the air bubble monitored in part b is indicated by the dashed circle and the arrow underneath the first image indicates the position of the profile given in part b. b) Profiles of T_2 relaxation time against sample height taken, in line with position of arrow, from the T_2 relaxation time maps in part a. A line is drawn for each profile indicating the position of the average T_2 value (T_2 = 540 ms). c) X-ray CT image of a vesicle-polymer mixture (ϕ = 0.5 [polymer] = 0.25 %wt) containing air bubbles.

The results, shown in figures 3 and 4, demonstrate that air bubbles can be trapped inside the depletion gel long enough to have an impact on the stability of vesicle-polymer mixtures. One of the effects of entrapped air bubbles is the increase in density difference between gel and continuum phases, thus, increasing the magnitude of gravitational forces.

Figure 5a shows photographs of a vesicle-polymer mixture (ϕ = 0.3, [polymer] = 0.25 %wt) before (t = 0) and after phase separation (t = 5 weeks (wk)). The photograph taken at (t = 5 wk) shows a transparent fluid at the base of the container underneath a cloudy blue region, which was attributed to the vesicle-poor and vesicle-rich phases, respectively. Vesicles, and their particularly aggregates, are slightly less dense than the continuous phase, so cream to the top of the sample. At t = 0, the T_2 MR relaxation maps (figure 5b) show the vesicle-polymer mixture is homogenous with an average T_2 = 540 ms. From t = 1 wk, regions of higher T_2 (T_2 > 600 ms) appear in the images that are associated with regions containing fewer vesicles. Initially, vesicle-poor regions only form close to the container walls and follow the shape of the container. After t = 3 wk, a vesicle-poor phase is also observed in the T_2 relaxation maps at the bottom of the tube. At this point phase separation could be observed visually.

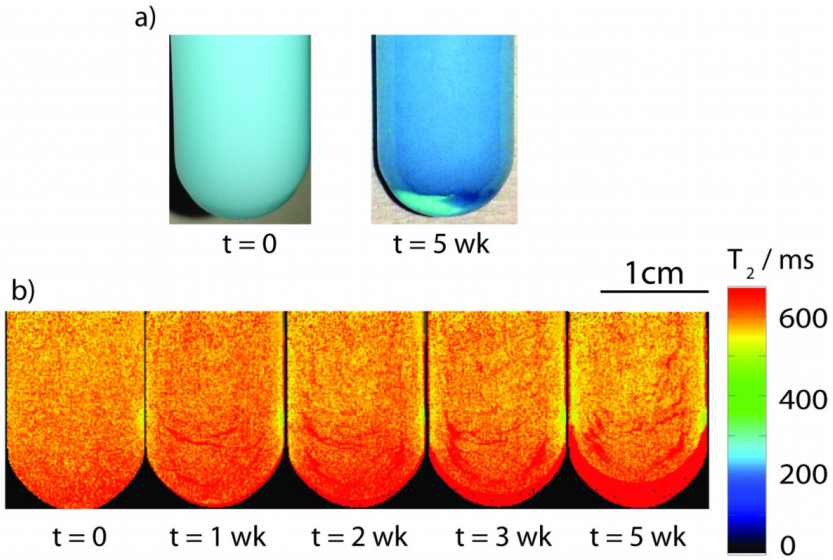

Figure 5: a) Photographs of a vesicle-polymer mixture (ϕ = 0.3, [polymer] = 0.25 %wt) at t = 0 and t = 5 wk. b) T_2 relaxation time maps of a vesicle-polymer mixture (ϕ = 0.3, [polymer] = 0.25 %wt) at t = 0 - 5 wk.

The failure model, to describe the phase separation observed in the images in figure 5, is reminiscent of the compression and collapse of colloidal gels and it can be attributed to the buoyancy force due to the presence of trapped air bubbles. In fact, while the X-ray CT image after 24 hours of a sample of this composition did not show evidence of trapped bubbles, it is possible that the presence of a few, small, undetected air bubbles were enough to induce compression in this weak gel. ($\sigma_0 \approx 0.02$ Pa).

3.3 Phase separation in samples produced under vacuum

In order to eliminate the effect of trapped air bubbles, samples were produced under vacuum and they showed, indeed, a completely different behavior from aerated samples. In particular, we did not observe, within the observation period, the formation of a large vesicle-poor region at the

bottom, which would be predicted for a poro-elastic compression, but we still see a microscopic phase separation with vesicles poor phases forming close to container walls, at the top of the sample vial or, later in time, in the bulk of the sample.

The effect on phase separation of changing vesicle volume fraction (Figure 6), at a constant polymer concentration (0.1 %wt) and changing polymer concentration (Figure 7) at a constant vesicle volume fraction ($\phi = 0.4$), was investigated over a period of 5 weeks. In figure 6, it can be seen that the T_2 relaxation time depends on the vesicle volume fraction. At $\phi = 0.5$, the average T_2 relaxation time is 530 ± 41 ms, and increases to 580 ± 36 ms at $\phi = 0.4$ and 630 ± 25 ms at $\phi = 0.3$. All samples, irrespective of volume fraction, show the development of regions of higher T_2 relaxation time, associated with regions of lower vesicle volume fraction, over the 5 wk period. In all samples, these vesicle poor regions are observed to develop close to the sides of the container and at the top of the sample, near the meniscus. It was found that the sample at $\phi = 0.4$ appears to phase separate more slowly than the other volume fractions, with many regions of higher T_2 appearing after 7 days, compared to 2 days for $\phi = 0.3$ and 0.5. However, a small region of high T_2 can be seen forming near the container walls in the axial images at $\phi = 0.4$ at t= 2 days.

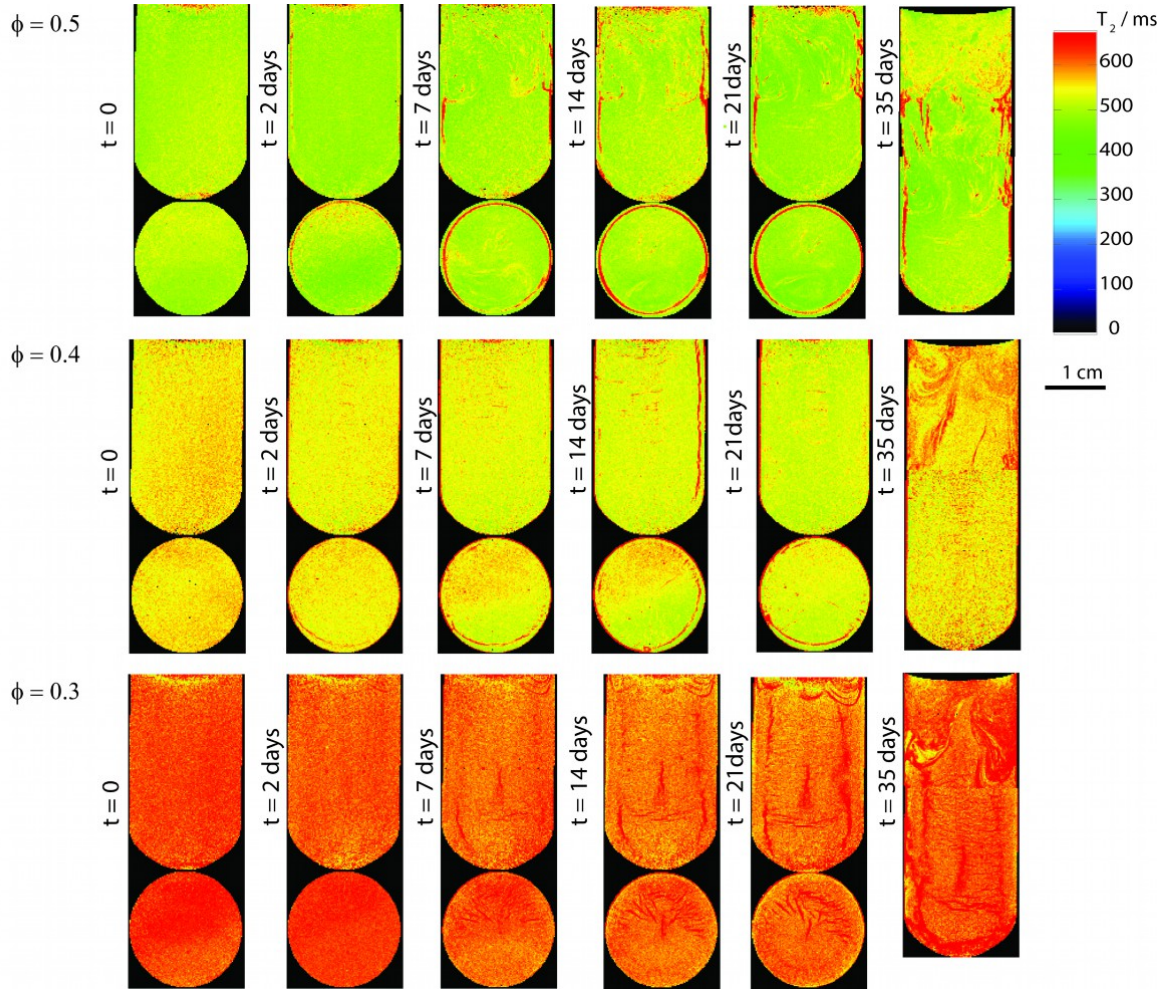

Figure 6: ^{1}H T_2 MR relaxation time maps of vesicle-polymer mixtures with polymer concentration = 0.1 %wt and $\phi = 0.5$, 0.4 and 0.3 over 5 weeks.

Figure 7 shows that the T_2 MR relaxation time for a vesicle-polymer mixture is also sensitive to polymer concentration, as well as vesicle volume fraction, with average T_2 relaxation times measured at 580 ± 36 ms (0 wt%), 550 ± 32 ms (0.05 wt%), 530 ± 44 ms (0.1 wt%), 490 ± 24 ms (0.15 wt%) and 470 ± 30 ms (0.25 wt%). The most stable sample appears to be the one without any polymer, which remains homogeneous over the 5 wk period. The remaining samples all show the emergence of regions of higher T_2 MR relaxation times, associated with vesicle poor regions, which appear close to the container edges and sample meniscus. The rate of phase separation appears to be slowest at a polymer concentration of 0.1 %wt, with this sample showing fewer regions of higher T_2 MR relaxation time, particularly at early time.

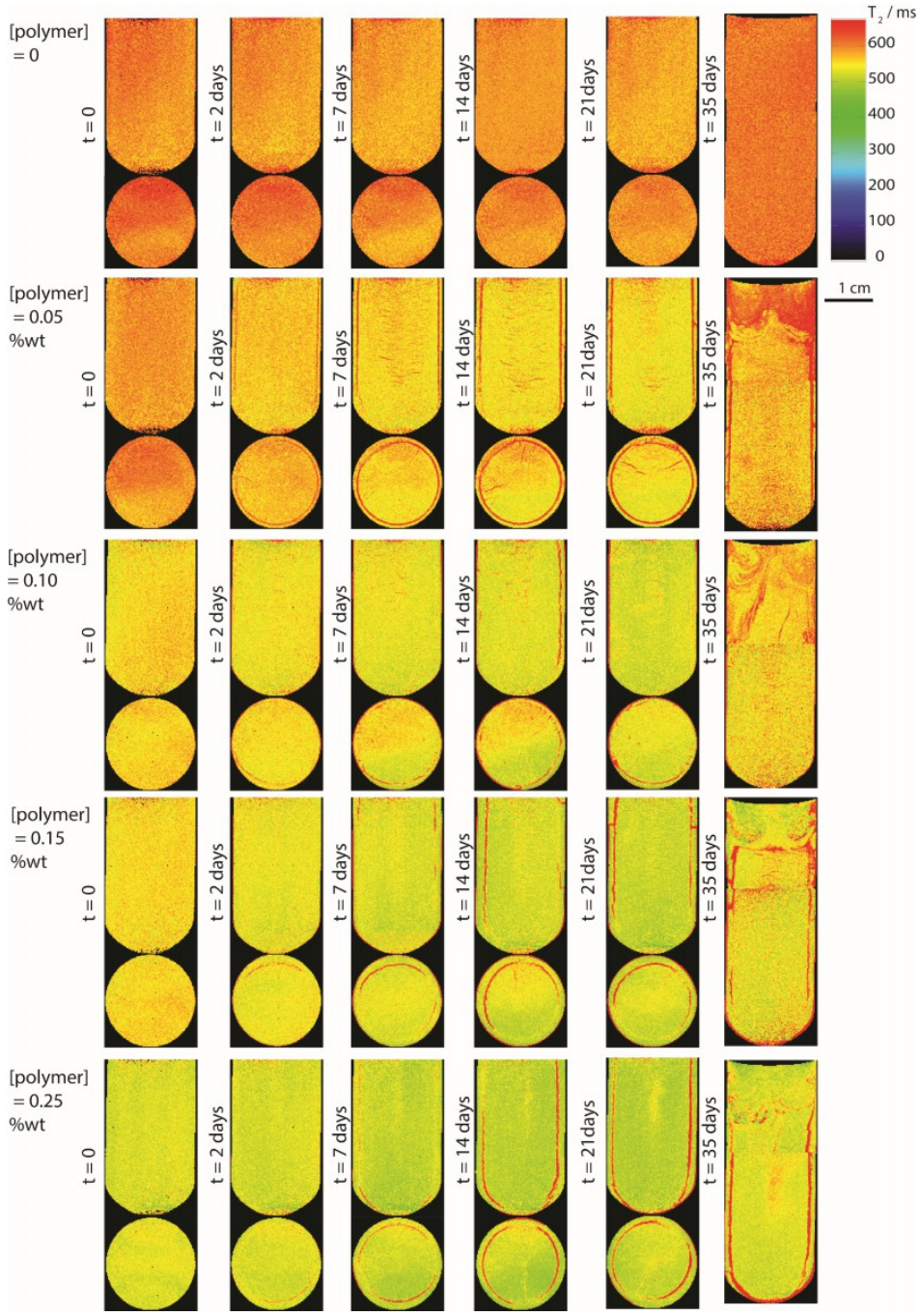

Figure 7: ^{1}H T_2 MR relaxation time maps of samples with polymer concentration = 0, 0.05, 0.10, 0.15 and 0.25 %wt and $\phi = 0.4$ over a 5 wk time period.

While it is possible to qualitatively assess the degree of phase separation from visual inspection of the images, Moran's I spatial autocorrelation is able to provide a quantification of the degree of phase separation [15]. Using Moran's I, the degree of phase separation was calculated for each image in Figures 6 and 7, which are plotted in Figure 8. In Figure 8a, it can be seen that Moran's I increases

more rapidly for samples at ϕ = 0.3 and ϕ = 0.5, indicating these samples phase separate faster. In Figure 8b, it can be seen that Moran's I increases most markedly from a value of 0.1 to 0.7 for the sample at polymer concentration = 0.25 %wt. The Moran's I value for mixtures at a polymer concentration of 0.05 - 0.15 %wt also increase, but by not as a great an extent as 0.25 %wt. The Moran's I value for the sample without polymer was found to remain around 0.2. The sample at a polymer concentration of 0.10 %wt was found to have the smallest increase in Moran's I value, for a sample containing polymer, which agrees with the qualitative observation that this sample phase separates slowest.

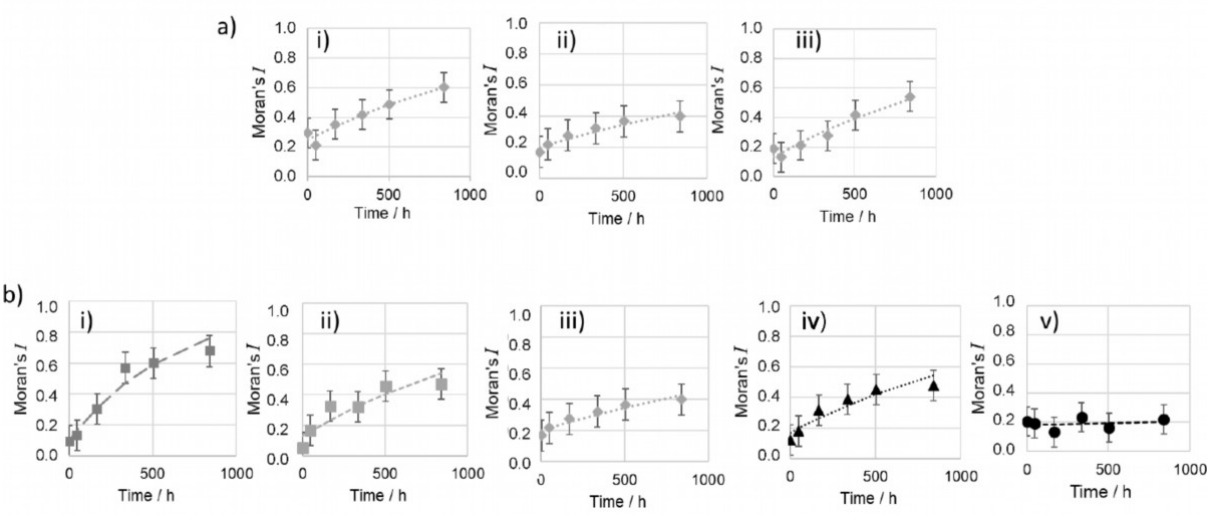

Figure 8: a) Plots of Moran's I against time for ϕ = 0.5 (i), 0.4 (ii) and 0.3 (iii) at polymer concentration = 0.10 %wt, b) Plots of Moran's I against time for polymer concentrations = 0.25 (i), 0.15 (ii), 0.10 (iii), 0.05 (iv) and 0.00 (v) %wt at ϕ = 0.4. Dotted lines show the fit to a first order rate equation [15].

Using the Moran's I values, the rate of phase separation was calculated and its dependence on polymer concentration is shown in Figure 9, as described in [15]. As expected from qualitative inspection of the MR images, the rate of phase separation is lowest for the sample which does not contain polymer. The rate of phase separation was found to increase with polymer concentration, apart from the sample with the lowest (0.05 %wt) polymer concentration, which was found to phase separate fastest. Figure 8 also shows the rate of phase separation at ϕ = 0.3 and ϕ = 0.5 for samples

with 0.10 %wt polymer, which indicates the rate of phase separation is slower at higher vesicle volume fraction.

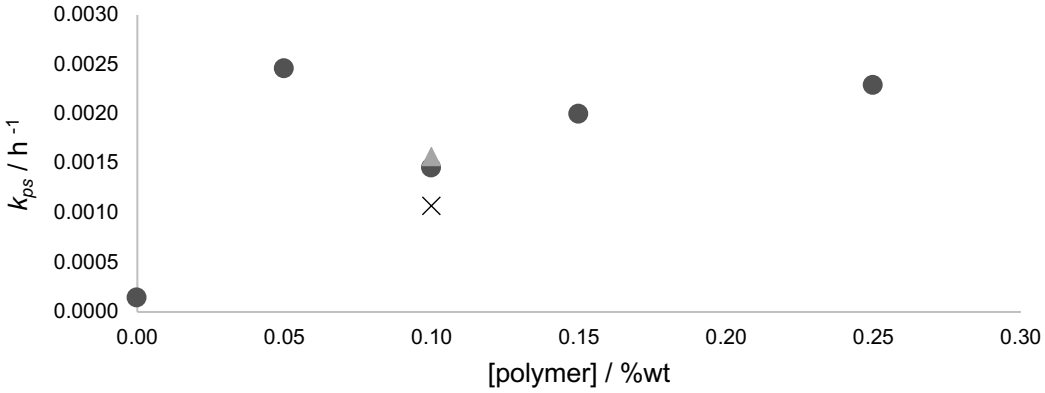

Figure 9: Plot of rate of phase separation vs polymer concentration for $\phi = 0.5$ (grey cross), 0.4 (black dots) and 0.3 (grey triangle)

Finally, Figure 10 shows the relationship between yield stress and the rate of phase separation. The graph shows that, at $\phi = 0.4$, stronger gels phase-separate more quickly. Higher vesicle volume fractions lead to stronger gels that separate more slowly. Only data from samples with yield stress > 0.005 Pa and images shown herein are displayed in Figure 10.

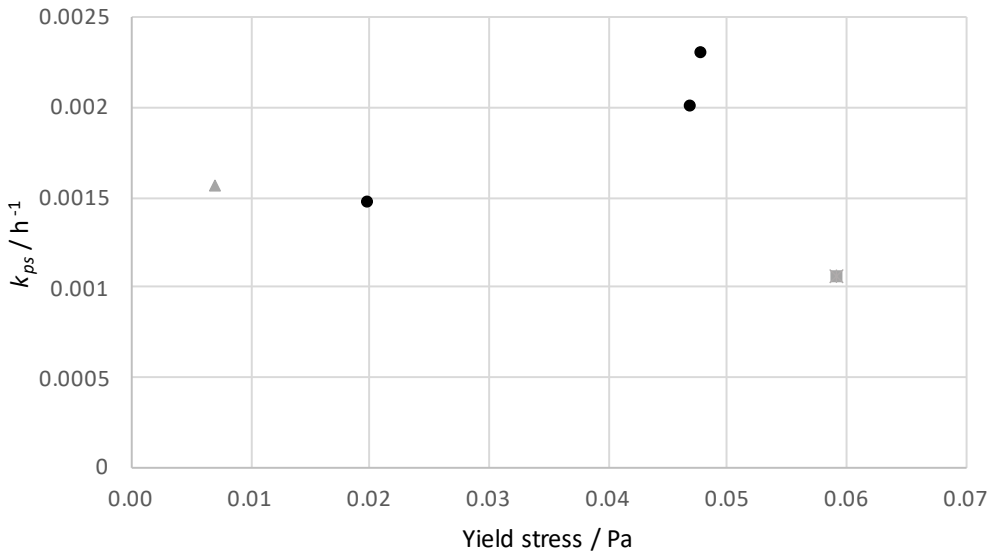

Figure 10: Plot of rate of phase separation vs yield stress for $\phi = 0.5$ [polymer] = 0.10 %wt (grey square), 0.4 [polymer] = 0.10, 0.15 and 0.25 %wt (black dots) and 0.3 [polymer] = 0.10 %wt (grey triangle). The relationship between yield stress and polymer concentration can be found in figure 2.

4. Discussion

In general, our systems tend to remain metastable for a much longer time than those previously investigated [3, 10]. This is probably due to the higher volume fraction, increasing crowding and smaller density mismatch in the systems studied herein. Aerated samples phase separate as expected for a density mismatched colloidal gel. It is apparent from a comparison of the photographs and MR images in Figures 4, 5, 6 and 7, that phase separation, in non-aerated vesicle-polymer mixtures, cannot be described by a poro-elastic model, and it can be identified significantly earlier by MRI than visual inspection. The MR images also reveal the development of regions of low vesicle concentration prior to phase separation in all cases.

The presence of air bubbles was found to have a significant impact on the stability of a sample as they rose through the network, due to gravity, disrupting the gel network and causing vesicle-poor cracks to form as they passed. The impact of air bubbles is twofold, not only does it induce gel compression/collapse, but it also accelerates the failure. Hence, the presence and lifetime of trapped air bubbles strongly influences the stability of these samples. We believe that air bubbles, which are trapped long enough, not only disrupt the network in a small localised region, but they increase the density difference between the gel vesicle-rich phase and the continuous polymer-rich aqueous phase. When air bubbles overcome yield stress and they move up, they are able to dig a tunnel in the network, the fact that the trajectory does not heal is a demonstration that the gel formed has a very long relaxation time. Furthermore, slow moving air bubbles create vesicle-poor regions increasing the colloidal gel porosity and this accelerates phase separation. This has previously been observed in iron oxide suspensions [37].

The lifetime of an air bubble trapped in the gel is dependent on the yield stress of the gel. An air bubble exerts a force on the gel network and if that force is greater than the gel's yield stress, the air bubble will be mobile [38, 39]. In the vesicle-polymer mixtures investigated here, the air bubbles are found to be mobile as shown in the MR images (Figure 4), and hence, the stress exerted by the air bubbles is greater than the yield stress. The minimum yield stress required to trap air bubbles of 300 μm indefinitely is 0.07 Pa, calculated from equations 4 and 5:

$$Y_g = \frac{2\,\pi\,\sigma_y\,R^2}{F} \qquad (4)$$

$$F = \frac{4}{3}\,\pi\,R^3\Delta\rho\,g \qquad (5)$$

where Y_g = 0.143 and is the dimensionless yield stress and takes into account size and shape of the yielded region [38, 40], R is the radius of the air bubble, $\Delta\rho$ is the density differences between the air bubble and the vesicle-polymer mixture and g the gravitational acceleration. The number and size of air bubbles trapped decreases as the polymer concentration and ϕ decrease (figure 3), because the gel strength (yield stress) decreases with decreasing polymer concentration and ϕ (figure 2). Modelling the yield stress data using equation 3 shows that gel strength is more dependent on polymer concentration than ϕ, as $\alpha > \beta$ and it would be possible, using equation 3, to predict whether specific polymer concentrations and values of ϕ would be able to trap air bubbles. However, the data do not fit the model perfectly. It has been found that DEEDMAC vesicles shrink when mixed with salt solutions or polymer solutions[15, 41-45]. Such shrinkage reduces the total volume fraction of the suspension and the resulting, reduced, vesicle volume fraction causes the model to not completely fit the data. This effect is most prominent for samples at high polymer concentration where the osmotic strength of the added material is highest. This shrinkage also results in a reduction in the T_2 relaxation time on polymer addition as is observed in figure 7 [15]. A reduction in the vesicle volume would also result in weaker gels as the smaller vesicles would not be able to span space as easily. Hence the polymer concentration has two counteracting effects on gel strength.

It was observed that, in non-aerated samples, the vesicle-poor regions form first close to the container walls (figure 6 and 7). There is currently no explanation for this. It could be a consequence of the preferential attraction between glass surface and charged cationic polymers, which creates a depletion layer for vesicles, or it could be a consequence of stress transmission in the network [6], or a combination of both.

Based on the poro-elastic model, it is expected that the formation of a stronger gel promotes greater stability, for a formulation, as the elastic gel supports vesicles against gravitational forces. However, in vesicle-polymer mixtures at lower ϕ and higher polymer concentration than used here the opposite has been shown [3, 10]. From the T_2 MR relaxation time maps in Figure 8, it can be observed that, at ϕ = 0.4, the stronger gels phase separate more quickly, which agrees with previous research [3, 10]. Yet, the gel at ϕ = 0.4 and polymer concentration = 0.05 %wt is found to separate more quickly than expected. In figure 6, it can also be seen that the gels at $\phi = 0.3$ appear to be more separated than those at higher volume fraction so it appears weaker gels are less stable. The increased rate of phase separation at low ϕ can be explained by the gel network being more tenuous, as the vesicles are less close packed. This leads to a more porous network, which has previously been shown to decrease gel stability [3, 10]. Furthermore, the unexpected increase in rate of phase separation at low polymer concentration has also been observed at $\phi = 0.5$ and $\phi = 0.3$ [30]. This could be because the interparticle forces are not sufficiently strong for a space spanning network to form, so loosely packed aggregates form [46]. These aggregates are mobile and less dense than the continuous water phase and, thus, accelerate phase separation. From figure 8, a quantitative assessment of the rate of phase separation can be made. The values of *k* calculated agree with the observations made visually. The graphs in figure 9 and figure 10 indicate that an optimum polymer concentration where phase separation is minimised might exist. It can be seen that a sample with high ϕ but a weak gel network,

so that it does not trap air bubbles, will be the most stable, similar to the sample at ϕ = 0.4 polymer concentration = 0.1 %. In general, the non-linear behaviour of rate of separation with volume fraction and polymer concentration is probably explained by the interplay between two different mechanisms: gravitational collapse and viscoelastic phase separation.

5. Conclusion

In colloidal systems with attractive interparticle forces, phase separation can be described as transient gelation and is often followed by consolidation due to gravity [1,2,3,5,6]. However, it has also been shown that phase separation can occur in the absence of a density difference, due to the depletion interaction [16, 17]. Phase separation in vesicle-polymer systems, particularly DEEDMAC vesicles mixed with polyDADMAC solution, have previously been described as separation by poro-elastic consolidation which describes transient gelation and collapse under gravity [3,10]. Herein, it has been shown that the mechanism of collapse in the vesicle-polymer mixture studied depends on the presence or absence of air bubbles.

In the presence of air bubbles, phase separation is a fast phenomenon, which follows poroelastic consolidation and is driven by density differences between the air bubbles and surrounding fluid. Investigations into vesicle-polymer systems with ϕ = 0.3 - 0.5 and polymer concentrations in the range 0 - 0.25 %wt showed that gels, at higher ϕ and polymer concentrations, are able to trap air bubbles. The ability to trap air bubbles depends on the yield stress of the gel formed. At yield stresses higher than 0.027 Pa, air bubbles were visualised, by X-ray CT, in the gel 24 h after mixing [30]. The effect of trapped air bubbles, on sample stability, was observed over time by MRI. The MR images showed vesicle-poor cracks forming in the wake of rising air bubbles revealing the direct relationship between air bubbles and the phase separation process. Formation of vesicle-poor cracks increases the porosity of the transient gel and increases the rate of phase separaiton [12]. While accelerated phase

separation has previously been observed in aerated systems [37], it is only by using MRI that this direct relationship can be observed in these turbid mixtures.

In the absence of air bubbles, phase separation is a slow process due to the small density difference between the vesicles and continuous phase. In these cases, phase separation can be described as viscoelastic phase separation, where the volume-shrinking of the transient gel is most likely driven by the depletion attraction between the vesicles [16,17]. In this system, MRI shows that the phase separation begins with very small vesicle-poor regions forming in the sample. These small cracks were observed weeks before phase separation became visually apparent. The formation of these cracks, close to the container walls, is consistent with volume shrinking of the transient gel [16,17]. The effect of composition and, therefore, gel strength on stability was quantified over large range of vesicle polymer mixtures, using Moran's I to quantify the rate and extent of phase separation [15]. It was found that strong and weak gels separated faster as did those with low ϕ. Faster separation, at higher gel strength, has been observed previously [3,10], but the results from these previous investigations cannot be directly compared with those herein. Previously the phase separation process was only studied by visual observation, so the samples likely contained undetected air bubbles. From the results presented in this paper, an optimum gel, in which phase separation is slowest, was found to have high ϕ and low gel strength. Such a sample is expected to be macroscopically stable for long periods of time.

Acknowledgments

The authors thank EPSRC (grants EP/M506461/1 and EP/K039245/1) for financial support**.**

Data Availability

The data generated in this study are available at https://doi.org/############## {DOI to be confirmed}

References

[1] P.J. Lu, D.A. Weitz, Colloidal Particles: Crystals, Glasses, and Gels, Annual Review of Condensed Matter Physics 4 (2013) 217-233.
[2] L. Starrs, W.C.K. Poon, D.J. Hibberd, M.M. Robins, Collapse of transient gels in colloid-polymer mixtures, Journal of Physics: Condensed Matter 14 (2002) 2485.
[3] J. Yeon Huh, M.L. Lynch, E.M. Furst, Poroelastic Consolidation in the Phase Separation of Vesicle-Polymer Suspensions, Ind. Eng. Chem. Res 30 (2011) 78-84.
[4] A. Caria, O. Regev, A. Khan, Surfactant–Polymer Interactions: Phase Diagram and Fusion of Vesicle in the Didodecyldimethylammonium Bromide–Poly(ethylene oxide)–Water System, J. Colloid Interface Sci., 200 (1998) 19-30.
[5] R. Harich, T.W. Blythe, M. Hermes, E. Zaccarelli, A.J. Sederman, L.F. Gladden, W.C.K. Poon, Gravitational collapse of depletion-induced colloidal gels, Soft Matter 12 (2016) 4300-4308.
[6] S. Manley, J.M. Skotheim, L. Mahadevan, D.A. Weitz, Gravitational Collapse of Colloidal Gels, Physical Review Letters 94 (2005) 218302.
[7] J.A. Yanez, E. Laarz, L. Bergström, Viscoelastic Properties of Particle Gels, Journal of Colloid and Interface Science 209 (1999) 162-172.
[8] R. Lipowsky, The conformation of membranes, Nature 349 (1991) 475-481.
[9] P. E. Hellberg, K. Bergstrom, K. Holmberg, Cleavable Surfactants, J. Surfactants Deterg 3 (2000) 81-91.
[10] J. Yeon Huh, M.L. Lynch, E.M. Furst, Microscopic structure and collapse of depletion-induced gels in vesicle-polymer mixtures, Physical Review E 76 (2007) 8.
[11] M.G. Basavaraj, N.L. McFarlane, M.L. Lynch, N.J. Wagner, Nanovesicle formation and microstructure in aqueous ditallowethylesterdimethylammonium chloride (DEEDMAC) solutions, J. Colloid Interface Sci. 429 (2014) 17-24.
[12] R. Buscall, L.R. White, The Consolidation of Concentrated Suspensions .1. The Theory of Sedimentation, Journal of the Chemical Society-Faraday Transactions I 83 (1987) 873-891.
[13] A. Miyajima, R. Inoue, E. Onishi, M. Miyake, R. Hyodo, Structural Viscosity Induced by Depletion Effect in Stable Vesicle Dispersion, Journal of Oleo Science 68 (2019) 837-845.
[14] S. Bobroff, R.J. Phillips, Nuclear magnetic resonance imaging investigation of sedimentation of concentrated suspensions in non-Newtonian fluids, Journal of Rheology 42 (1998) 1419-1436.
[15] E.S. Thompson, P. Saveyn, M. Declercq, J. Meert, V. Guida, C.D. Eads, E.S.J. Robles, M.M. Britton, Characterisation of heterogeneity and spatial autocorrelation in phase separating mixtures using Moran's I, Journal of Colloid and Interface Science 513 (2018) 180-187.
[16] T. Koyama, H. Tanaka, Volume-shrinking kinetics of transient gels as a consequence of dynamic interplay between phase separation and mechanical relaxation, Phys. Rev. E 98 (2018).
[17] H. Tanaka, T. Araki, Simulation method of colloidal suspensions with hydrodynamic interactions: Fluid particle dynamics, Phys. Rev. Lett. 85 (2000) 1338-1341.
[18] A. Abeynaike, A.J. Sederman, Y. Khan, M.L. Johns, J.F. Davidson, M.R. Mackley, The experimental measurement and modelling of sedimentation and creaming for glycerol/biodiesel droplet dispersions, Chemical Engineering Science 79 (2012) 125-137.
[19] J. Acosta-Cabronero, L.D. Hall, Measurements by MRI of the settling and packing of solid particles from aqueous suspensions, AIChE Journal 55 (2009) 1426-1433.

[20] S.D. Beyea, S.A. Altobelli, L.A. Mondy, Chemically selective NMR imaging of a 3-component (solid–solid–liquid) sedimenting system, Journal of Magnetic Resonance 161 (2003) 198-203.
[21] E.V. Morozov, O.N. Martyanov, Probing Flocculant-Induced Asphaltene Precipitation via NMR Imaging: from Model Toluene-Asphaltene Systems to Natural Crude Oils, Applied Magnetic Resonance (2015) 1-13.
[22] E.V. Morozov, O.V. Shabanova, O.V. Falaleev, MRI Comparative Study of Container Geometry Impact on the PMMA Spheres Sedimentation, Applied Magnetic Resonance 44 (2013) 619-636.
[23] Y. Onuki, C. Funatani, T. Yokawa, Y. Yamamoto, T. Fukami, T. Koide, Y. Obata, K. Takayama, Magnetic Resonance Imaging of the Phase Separation in Mixed Preparations of Moisturizing Cream and Steroid Ointment after Centrifugation, Chemical & Pharmaceutical Bulletin 63 (2015) 377-383.
[24] M.A. Turney, M.K. Cheung, R.L. Powell, M.J. McCarthy, Hindered settling of rod-like particles measured with magnetic resonance imaging, AIChE Journal 41 (1995) 251-257.
[25] Z. Wuxin, J. Martins, P. Saveyn, R. Govoreanu, K. Verbruggen, T. Ariën, A. Verliefde, P. Van der Meeren, Sedimentation and resuspendability evaluation of pharmaceutical suspensions by low-field one dimensional pulsed field gradient NMR profilometry, Pharmaceutical Development and Technology, 18 (2013) 787-797.
[26] M. Seth, A. Ramachandran, L.G. Leal, Dilution Technique To Determine the Hydrodynamic Volume Fraction of a Vesicle Suspension, Langmuir 26 (2010) 15169-15176.
[27] F. Corominas, K. Quan, Y. Yang, K. Peers, Method of producing a fabric softening composition, U.S. patent (2013) US8759278B2.

[28] J. Hennig, A. Naureth, H. Friedburg, RARE imaging: a fast imaging method for clinical MR, Magn. Reson. Med. 3 (1986) 823-833.
[29] Prospa, Magritek, Wellington, New Zealand.
[30] E.S. Thompson, Magnetic Resonance Investigations of phase separation in Vesicle-Polymer Mixtures, School of Chemistry, University of Birmingham, 2019.
[31] P.A.P. Moran, Notes on Continuous Stochastic Phenomena, Biometrika 37 (1950) 17-23.
[32] MatLab, The MathWorks Inc., Natick, MA, 2000.
[33] C.A. Schneider, W.S. Rasband, K.W. Eliceiri, NIH Image to ImageJ: 25 years of image analysis, Nat Meth 9 (2012) 671-675.
[34] G. Mullineux, Non-linear least squares fitting of coefficients in the Herschel–Bulkley model, Applied Mathematical Modelling 32 (2008) 2538-2551.
[35] P. Saveyn, P. Van der Meeren, M. Zackrisson, T. Narayanan, U. Olsson, Subgel transition in diluted vesicular DODAB dispersions, Soft Matter 5 (2009) 1735-1742.
[36] L.C. Hsiao, R.S. Newman, S.C. Glotzer, M.J. Solomon, Role of isostaticity and load-bearing microstructure in the elasticity of yielded colloidal gels, Proceedings of the National Academy of Sciences 109 (2012) 16029-16034.
[37] G.G. Glasrud, R.C. Navarrete, L.E. Scriven, C.W. Macosko, Settling behaviors of iron oxide suspensions, AIChE Journal 39 (1993) 560-568.
[38] M. Beaulne, E. Mitsoulis, Creeping motion of a sphere in tubes filled with Herschel–Bulkley fluids, Journal of Non-Newtonian Fluid Mechanics 72 (1997) 55-71.
[39] S. Mirzaagha, R. Pasquino, E. Iuliano, G. D'Avino, F. Zonfrilli, V. Guida, N. Grizzuti, The rising motion of spheres in structured fluids with yield stress, Phys. Fluids 29 (2017) 093101.
[40] A.N. Beris, J.A. Tsamopoulos, R.C. Armstrong, R.A. Brown, Creeping motion of a sphere through a Bingham plastic, Journal of Fluid Mechanics 158 (2006) 219-244.
[41] C. Groth, J. Bender, M. Nyden, Diffusion of water in multilamellar vesicles of dialkyl and dialkyl ester ammonium surfactants, Colloids and Surfaces a-Physicochemical and Engineering Aspects 228 (2003) 64-73.
[42] C. Groth, K. Tollgerdt, M. Nyden, Diffusion of solutes in highly concentrated vesicle solutions from cationic surfactants - Effects of chain saturation and ester function, Colloids and Surfaces a-Physicochemical and Engineering Aspects 281 (2006) 23-34.

[43] P. Sabatino, P. Saveyn, J.C. Martins, P. Van der Meeren, Enclosed Volume Determination of Concentrated Dioctadecyldimethylammonium Chloride (DODAC) Vesicular Dispersions by Low-Resolution Proton NMR Diffusometry and T-2 Relaxometry, Langmuir 27 (2011) 4532-4540.
[44] P. Saveyn, J. Cocquyt, P. Bomans, P. Frederik, M. De Cuyper, P. Van der Meeren, Osmotically induced morphological changes of extruded dioctadecyldimethylammonium chloride (DODAC) dispersions, Langmuir 23 (2007) 4775-4781.
[45] P. Saveyn, J. Cocquyt, M. Gradzielski, P. Van der Meeren, Osmotic effects on the enclosed volume and interlamellar spacing of multilamellar DODAC vesicles, Colloids and Surfaces a-Physicochemical and Engineering Aspects 319 (2008) 62-70.
[46] H.N.W. Lekkerkerker, W.C.K. Poon, P.N. Pusey, A. Stroobants, P.B. Warren, Phase-Behavior of Colloid Plus Polymer Mixtures, Europhys Lett 20 (1992) 559-564.